New Journal of Physics
The open access journal at the forefront of physics

Deutsche Physikalische Gesellschaft DPG
IOP Institute of Physics

Published in partnership with: Deutsche Physikalische Gesellschaft and the Institute of Physics

OPEN ACCESS

RECEIVED
27 July 2016

REVISED
18 October 2016

ACCEPTED FOR PUBLICATION
9 November 2016

PUBLISHED
2 February 2017

PAPER

Anomalous electromagnetic coupling via entanglement at the nanoscale

Gregory Slepyan[1], Amir Boag[1], Vladimir Mordachev[2], Eugene Sinkevich[2], Sergey Maksimenko[3], Polina Kuzhir[3], Giovanni Miano[4], Mikhail E Portnoi[5] and Antonio Maffucci[6]

[1] School of Electrical Engineering, Tel Aviv University, Tel Aviv, Israel
[2] EMC R&D Lab., Belarusian State University of Informatics and Radioelectronics Minsk, Belarus
[3] Research Institute for Nuclear Problems of Belarusian State University, Minsk, Belarus
[4] Dept. of Electrical Engineering and Information Technology, University of Naples Federico II, Naples, Italy
[5] School of Physics, University of Exeter, Stocker Road, Exeter EX4 4QL, UK
[6] Dept. of Electrical and Information Engineering, University of Cassino and Southern Lazio, Cassino, Italy and National Institute for Nuclear Physics, INFN, LNF Frascati, Italy

E-mail: gregory_slepyan@yahoo.com

Keywords: quantum entanglement, electromagnetic coupling, crosstalk, generalized susceptibility, electromagnetic compatibility

Abstract

Understanding unwanted mutual interactions between devices at the nanoscale is crucial for the study of the electromagnetic compatibility in nanoelectronic and nanophotonic systems. Anomalous electromagnetic coupling (crosstalk) between nanodevices may arise from the combination of electromagnetic interaction and quantum entanglement. In this paper we study in detail the crosstalk between two identical nanodevices, each consisting of a quantum emitter (atom, quantum dot, etc), capacitively coupled to a pair of nanoelectrodes. Using the generalized susceptibility concept, the overall system is modeled as a two-port within the framework of the electrical circuit theory and it is characterized by the admittance matrix. We show that the entanglement changes dramatically the physical picture of the electromagnetic crosstalk. In particular, the excitation produced in one of the ports may be redistributed in equal parts between both the ports, in spite of the rather small electromagnetic interactions. Such an anomalous crosstalk is expected to appear at optical frequencies in lateral GaAs double quantum dots. A possible experimental set up is also discussed. The classical concepts of interference in the operation of electronic devices, which have been known since the early days of radio-communications and are associated with electromagnetic compatibility, should then be reconsidered at the nanoscale.

1. Introduction

The idea of quantum entanglement appears in two famous paradoxes of quantum theory (Schrödinger's cat paradox [1] and the paradox of Einstein–Podolsky–Rosen [2]). For many years entanglement was of special interest in the context of experimental studies aimed at proving the completeness of quantum mechanics and the feasibility of quantum measurements [3]. Dicke introduced in 1954 the concept of super-radiance [4], which involves the collective states, currently known as Dicke-states. These states turned out to be highly entangled. Scully and co-workers focused on the problem of a single photon stored in a dense cloud of atoms whose linear dimensions are large compared with the wavelength of light [5–13]. The atoms in various positions are excited at different moments in time (Dicke-states timing) and the usual picture of super-radiance is no longer valid due to the photonic delay. In this case, peculiar features of the cooperatively emitted radiation have been predicted. In particular, a single photon absorbed by a cloud of N atoms is followed by a spontaneous emission in the same direction [6]. Another important mechanism corresponds to the presence of two excited atoms inside the cloud and one virtual photon with 'negative' energy [5]. As shown in [5], the virtual photons produce a collective Lamb-shift, which has been experimentally observed in [14, 15]. A recent step forward was taken in [13], where

some distinctive properties of super-radiance in the lattices have been predicted. This gave birth to what is known today as 'correlated spontaneous emission'. This effect was proposed as a basis for operation of some types of quantum optical nanoantennas [16, 17].

The present-day developments in nanotechnologies make entanglement phenomena relevant for the proper operation of nanoelectronic devices and systems. Recently, quantum entanglement was identified to be a very useful tool facilitating the growth in the level of integration and the reduction of the operation power in nanoelectronics and nano-optics. Among the promising devices based on entanglement are quantum qubits of various types [18–21] and quantum amplification by superradiant emission of radiation (QASERs) [22].

On the other hand, this trend enhances the role of the dense and highly integrated environment in the behavior of individual nanodevices. Similar problems, associated with Electromagnetic Compatibility (EMC), have been known since the early days of radio-communications, where 'unwanted' generation of electromagnetic fields causes interference in electrical and electronic devices [23–25]. Such electromagnetic coupling is associated with crosstalk—a mutual interaction among neighboring devices via near field penetration from one to another—is probably the most notable manifestation of such an interference [23–25]. Citing [24]: 'This essentially refers to the unintended electromagnetic coupling between wires and printed circuit boards (PCB) lands that are in close proximity. Crosstalk is distinguished from antenna coupling in that it is a near-field coupling problem. Crosstalk between wires in cables or between lands on PCBs concerns the intrasystem interference performance of the product; that is, the source of the electromagnetic emission and the receptor of this emission are within the same system'.

The progress in nanoelectronics is accompanied by a general trend towards the application of radio-communication principles to the optical frequency range, and thus intricate mechanisms of interference emerge on the nanoscale [26–28]. In fact, lumped electric circuits and segments of single-mode transmission lines became commonly used elements in high-frequency applications, including optical devices [29, 30]. Optical coherent sources are characterized by overlapping frequency spectra, which contribute to often undesirable mutual interactions that can be classified as one of the types of optical EMC problems [31–37]. Another type of EMC problem appears when different types of nanoantennas are located in close proximity to strongly reflecting surfaces of photonic crystals and plasmonic metals [31, 33, 38–40]. Thus, the definition of crosstalk cited above, is adequate for nanoelectronics and will be used in the remainder of the paper for conciseness.

The electromagnetic interference on the nanoscale due to the high density of components may be accompanied by the formation of an undesirable quantum entanglement, and as a consequence the qualitative picture of crosstalk may be dramatically changed. Being a mechanism of quantum interference [3], entanglement can produce a combined 'electromagnetic-quantum' crosstalk and induce long-distance and long-living electrical correlations. Such a long-distance entanglement was experimentally observed in [15] on a set of trapped ions at inter-ion separations that are much larger than the wavelength of the resonant transition. As a result, an electric crosstalk becomes anomalously high even for rather weak mutual field penetration. The entanglement manifestation in nanocircuits can be strongly influenced by various types of environmental elements, *e.g.,* resonant cavities [41] and waveguides near cutoff [42]. Another significant external influence might be due to the non-linear inter-circuit interactions, produced by strong additional fields. Among such effects are the laser induced dipole-dipole interactions [43], which correspond to the resonant inter-dipolar interaction in any confined geometry. The role of these effects in nano-EMC can be dual. Depending on the system parameters, they are able to open additional unwanted channels of anomalous crosstalk. On the other hand, they can provide promising tools for electromagnetic crosstalk suppression. Examples of both types will be discussed below.

Consequently, in view of the electromagnetic-quantum crosstalk, classical EMC concepts like coupling, shielding, and matching, should be reconsidered with respect to nanodevices. For this reason, the conventional EMC-language (electrical circuit theory) should be combined with quantum mechanics and quantum optics. Different variants of circuit theory with respect to some types of nanodevices were recently discussed [22, 40, 44–49]. For EMC-applications, we need a universal concept of nanocircuits that are composed of multiports of various types. Such a concept may be developed on the basis of the theory of general susceptibilities [50, 51]. The elements of admittance matrices belong to the class of kinetic coefficients, which obey general Onsager symmetry rules [51] and are calculated via the Kubo technique. Parameters such as an effective complex admittance are measurable characteristics of nanoelements [48, 49]. Effects of decoherence may be taken into account through phenomenological models basing on the concept of quasi-discrete levels [52] with the values of phase relaxation times taken from the experimental data [47, 53].

To illustrate these topics, we study in detail the crosstalk between two quantum emitters, e.g., quantum dots (QD), polar molecules, etc, in an electrical circuit. Speaking about a quantum emitter as an element of an electrical circuit, we mean that it is placed between the ends of two nanoelectrodes, to which it is strongly capacitively coupled, see figure 1. The electrodes play the role of interconnects linking the quantum emitters with the other elements of the circuit. The two quantum emitters are in entangled states and are directly coupled

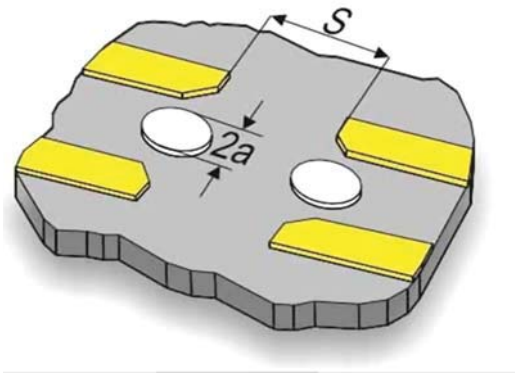

Figure 1. Two quantum emitters in an electrical circuit: each emitter is capacitively coupled to an electrode pair through which it is connected to the circuit; a is the emitter radius and S is the distance between the electrode pairs.

via the dipole-dipole (d-d) interaction, whereas the two pairs of electrodes are directly coupled capacitively. The overall system is represented as an electrical two-port, and it is characterized in terms of its admittance matrix. We find that the combination of the d–d interaction and the entanglement give rise to an anomalous crosstalk between the two nanodevices.

The paper is organized as follows. In section 2 an equivalent two-port of the two coupled quantum emitters in entangled states is proposed. In section 3 the anomalous electromagnetic crosstalk arising from the entanglement is investigated and compared with the classical case. Furthermore, an experimental setup is proposed, to observe the anomalous electromagnetic crosstalk via entanglement in a system with a pair of coupled lateral GaAs quantum dots. Summary and outlook are formulated in section 4.

2. Equivalent electrical two-port of a pair of quantum emitters in entangled states

Speaking of a quantum emitter as an element of an electrical circuit, we mean that it is placed between the ends of two electrodes (figure 1), to which it is strongly capacitively coupled; a is the linear size of the quantum confinement area of each quantum emitter and S is the distance between two emitters. Assuming strong coupling means that the electric field surrounding the electrodes strongly penetrates the quantum emitter. Therefore, absorption and spontaneous emission of the charge carrier (electron-hole pair, exciton, etc) from the electrodes by the quantum emitter represents the main mechanism of its transition to the excited state and vice-versa. From the qualitative point of view, this process appears as tunneling of the charge carriers through the quantum emitter.

A quantum emitter has been proposed as an element of a spin qubit for quantum computing [36]. It corresponds to a lateral QD of a heterostructure, with the confinement of a two-dimensional electron gas produced by the electric gates on the surface. The electrostatic gates can, in addition, drive the electron dynamics by an ac-potential, resulting in an ac-current excitation in the QD: the ac-current is produced by the quantum interband transition between the valence and conduction bands. This QD may be represented as a 2D-quantum harmonic oscillator whose energy spectrum and eigenstates are described by the Fock–Darwin model [37]. In the following, for brevity, we refer to the quantum emitter as an 'atom' regardless of its physical nature.

The equivalent electrical two-port for the system in figure 1 depends on its quantum state. The first step made by Greffet *et al* in [44] involves a single quantum emitter initially prepared in the ground state and placed inside a micro-cavity or near a nano-antenna. In this section, we first review the one-port model proposed in [44] for a single quantum emitter and then we generalize it to a system of two quantum emitters in entangled states coupled via the d-d interaction.

2.1. Single quantum emitter

By following Greffet *et al* [44] the electromagnetic behavior of a single quantum emitter (figure 2(a)) is described through a one-port element characterized by the 'effective impedance' $Z_e(\omega)$: Z_e is the ratio between the voltage V between the electrodes and the induced current I, both defined at the electrical 'port', i.e. the cross section indicated in figure 2(b). We consider a two-level atom with a ground state $|g\rangle$ and an excited state $|e\rangle$ (figure 2(c)). Assuming a time dependence in the form $\exp(-i\omega t)$, we obtained the following effective impedance for the atom prepared in the ground state $|g\rangle$ (for details see appendix A):

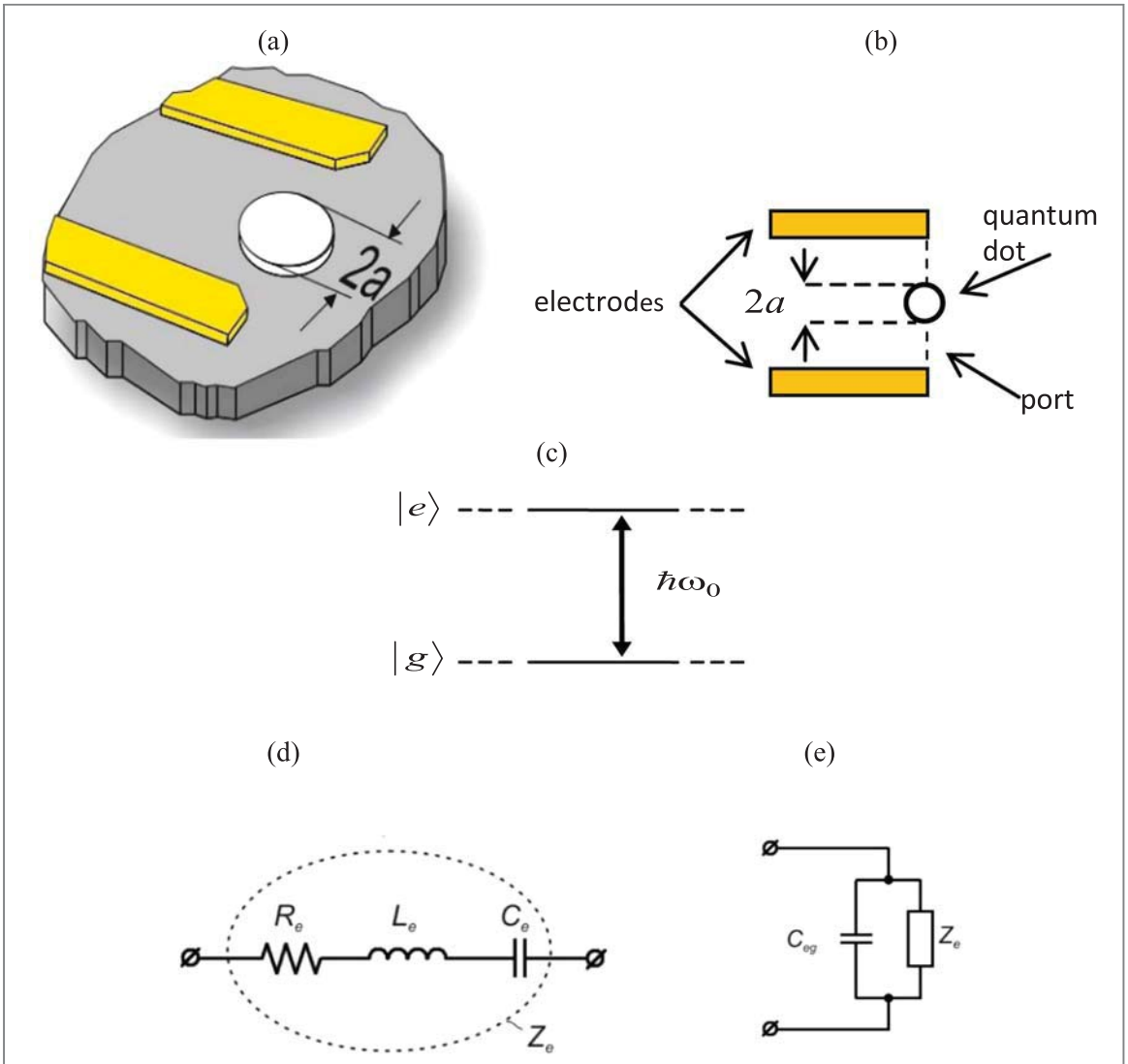

Figure 2. A single quantum emitter coupled to two electrodes: (a) the quantum emitter is coupled capacitively to the two electrodes, which drive the electron dynamics by an applied ac-voltage; (b) transverse section at which the electrical port is defined; (c) two-level model of the quantum emitter; (d) equivalent RLC series one-port of the single quantum emitter; (e) equivalent impedance of the emitter and electrodes: Z_e is in parallel with the inter-electrode capacitance C_{eg}.

$$Z_e(\omega) = \mathrm{i}\hbar\frac{\omega_0^2 - \omega^2 - \mathrm{i}\omega\gamma}{2\mu^2\omega\omega_0}A_{\mathrm{eff}}, \tag{1}$$

where $\mu = |\vec{\mu}|$ is the dipole moment of the transition, ω_0 is the frequency of the transition, γ is the decay rate of the excited level, A_{eff} is the effective area of quantum confinement and $\hbar$ is the Planck constant. The width of the resonance line may be efficiently controlled through the two electrodes (the Purcell-effect [54, 55]). The effective impedance (1) is rewritten as:

$$Z_e(\omega) = R_e - \mathrm{i}\omega L_e - \frac{1}{\mathrm{i}\omega C_e}, \tag{2}$$

which represents the impedance of an RLC series one-port (see figure 2(d)) where:

$$L_e = \frac{\hbar A_{\mathrm{eff}}}{2\mu^2\omega_0}, \quad R_e = \gamma L_e, \quad C_e = \frac{1}{\omega_0^2 L_e}. \tag{3}$$

The equivalent one-port of the system composed of the atom and two electrodes is shown in figure 2(e), where the impedance of the single emitter, $Z_e(\omega)$, is put in parallel with the capacitance of the electrode pair, C_{eg}.

2.2. Two quantum emitters

The electromagnetic behavior of the system in figure 1 is described by representing the two quantum emitters with the two pairs of electrodes as a two-port element; the sections where the ports are defined are indicated in figure 3(a). The two quantum emitters are coupled via d-d interactions and interact with classical

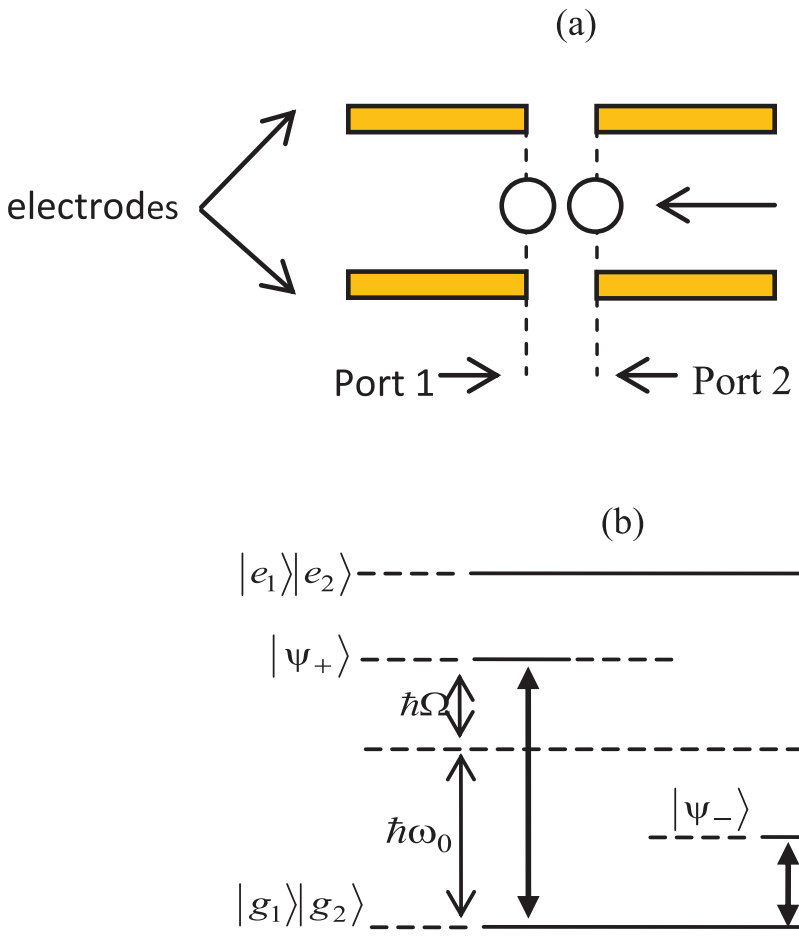

Figure 3. Equivalent electric two-port for the system in figure 1: (a) definition of the two ports; (b) the four-level model: $|g_1\rangle|g_2\rangle$ is the doubly ground state, $|\psi_+\rangle$ is the singly-excited symmetric (superradiant) state, $|\psi_-\rangle$ is the singly-excited anti-symmetric (subradiant) state, and $|e_1\rangle|e_2\rangle$ is the doubly excited state.

monochromatic electromagnetic field $\mathbf{E} = \mathrm{Re}\{\mathbf{E}_0 \exp(-\mathrm{i}\omega t)\}$. The physical mechanism of this coupling is via the inter-atomic exchange by the virtual photon over the common photonic bath [21, 56–58]. We assume that the external field is adiabatically switched on at a sufficiently early moment of time and the system is initially prepared in the ground state $|g_1, g_2\rangle$.

Assuming also that the system is asymptotically stable, the transient processes have completely decayed, and the system dynamics is reduced to stationary oscillations at the frequency of the external field. This system is described by an effective Hamiltonian $\hat{H} = \hat{H}_a + \hat{H}_{dd} + \hat{H}_{\mathrm{int}}$, where $\hat{H}_a = \hbar(\omega_0 - \mathrm{i}\gamma/2)\sum_{j=1,2}\hat{\sigma}_{jz}/2$ is the atomic component with $\hat{\sigma}_{jz}$ being the inversion Pauli matrix for the j-th atom, and γ is the radiative decay rate of the atomic transition. The second term, $\hat{H}_{dd} = \hbar(\Omega - \mathrm{i}\gamma_{12}/2)(\hat{\sigma}_1^+\hat{\sigma}_2^- + \mathrm{H.c.})$, is the interatomic component, where Ω is the collective Lamb shift, γ_{12} is responsible for cooperative radiative decay, $\hat{\sigma}_j^{\pm}$ are the creation-annihilation operators for the excited state in the jth atom (see appendix B). The last term in the Hamiltonian describes the atom-field interaction and is given by $\hat{H}_{\mathrm{int}} = -e\sum_{j=1,2}(\vec{\mu}\cdot\mathbf{E}_j)(\hat{\sigma}_j^+ + \hat{\sigma}_j^-)$ where $\mathbf{E}_j$ is the field value at the location of the j-th atom. The first two components of the effective Hamiltonian are non-Hermitian due to the presence of radiative losses. The radiative losses do not lead to attenuation, but define the widths of the resonance lines.

Let us assume, that the system interacts with the external field in the regime of weak coupling (the term $\hat{H}_{\mathrm{int}}$ should be considered as a small perturbation). Weak coupling (linear response) theory is based on the correct set of zero-order states (eigenstates of Hamiltonian $\hat{H} = \hat{H}_a + \hat{H}_{dd}$, satisfy the conditions of symmetry or anti-symmetry). The model under consideration corresponds to the narrowband weak field and covers a large number of practically interesting applications. In the broadband case, for example involving digital signals, the resonance conditions may be fulfilled for a large number of quantum transitions and may entangle the corresponding quantum states, whereby the two-level model becomes questionable. For strong fields, it is necessary to account for the nonlinear coupling effects via harmonic generation, Rabi-oscillations [54, 55] etc, thus, Kubo-approach breaks down.

The 'singly excited states' due to the entanglement and energy splitting are changed to the Dicke states [54, 55, 58]:

$$|\psi_+\rangle = \frac{1}{\sqrt{2}}(|e_1\rangle|g_2\rangle + |e_2\rangle|g_1\rangle), \tag{4}$$

and

$$|\psi_-\rangle = \frac{1}{\sqrt{2}}(|e_1\rangle|g_2\rangle - |e_2\rangle|g_1\rangle), \tag{5}$$

with respect to the eigen-states of the non-interacting atoms $|e_1\rangle|g_2\rangle$ and $|g_1\rangle|e_2\rangle$. These appear in addition to the ground $|g_1\rangle|g_2\rangle$ and doubly-excited $|e_1\rangle|e_2\rangle$ states, thus forming the four-level system represented in figure 3(b). The state (4) corresponds to the wavefunction that is symmetric with respect to the transposition of the atoms, and is referred to as the 'superradiant' state. The state (5) denotes the case of antisymmetric wavefunction and it is named the 'subradiant' state [55].

Superradiant and subradiant states are different in terms of their resonance frequencies $\omega_\pm$ and decay rates $\gamma_\pm = \gamma \pm \gamma_{12}$, where γ_{12} is given in appendix B (equation (B.8)). The resonance frequencies, $\omega_\pm = \omega_0 \pm \Omega$, are split by the doubled value of the collective Lamb-shift [55] due to the d-d interaction,

$$\Omega = \frac{\mu^2\omega_0^3}{2\pi\varepsilon_0 c^3\hbar}\left\{\left[\frac{\cos x}{x^3} + \frac{\sin x}{x^2} - \frac{\cos x}{x}\right] + \cos^2\theta\left[\frac{\cos x}{x} - \frac{3\cos x}{x^3} - \frac{3\sin x}{x^2}\right]\right\}, \tag{6}$$

where $\cos^2\theta = (\vec{\mu}\cdot\mathbf{r}_{12}/\mu\,|\mathbf{r}_{12}|)^2$, $\mathbf{r}_{12}$ is the inter-atomic radius vector, $|\mathbf{r}_{12}|$ is the inter-atomic distance, $x = \omega_0\,|\mathbf{r}_{12}|/c$, and c is the speed of light in vacuum.

We now characterize the two-port when the two-atom system, initially prepared in the ground state, is excited by a monochromatic electromagnetic field with frequency $\omega \approx \omega_0$. The interaction process is described by a three-level V-model, in which only the transitions between the ground state, $|g_1g_2\rangle$ and the above Dicke states (4), (5) are taken into account. The transition between the two Dicke states is forbidden and the transition between the ground and the doubly excited state is disregarded because it is not resonant (the resonance condition for this case is $\omega \approx 2\omega_0$). The three-level V-model is valid also for the initial state in the form of an arbitrary coherent superposition of superradiant and subradiant states in the regime of dipole blockade [59, 60]. The dipole blockade effect is defined as a strong d-d interaction of the two atoms in the $|e_1e_2\rangle$ state. It is defined via additional component in the d-d Hamiltonian, which is $\hat{H}_{\mathrm{Dipole-blockade}} = \hbar\delta|e_1e_2\rangle\langle e_1e_2|$ [59, 60]. This interaction forces are of the Foerster origin and vary with inter-atomic distance as $|\mathbf{r}_{12}|^{-6}$ [59, 60]. It results in a frequency shift δ of this doubly excited state, whereby the transitions to it from the Dicke states become non-resonant. The values of the frequency shift needed for the dipole blockade are sufficiently large to avoid resonant interactions with the $|e_1e_2\rangle$ state. This effect was recently observed experimentally in [61, 62].

Two voltages $V_{1,2}$ applied to ports 1 and 2 (see figure 3(a)) are identified with the electric fields $\mathbf{E}_{1,2}$, which act on the first and second emitters. Such fields play the roles of 'generalized forces', and the corresponding responses are identified with the displacement currents $I_{1,2}$ (this physical picture corresponds to that in [44] for single atom). Such currents may be related to voltages $V_{1,2}$ by introducing an admittance matrix, which due to the symmetry can be written as:

$$\begin{pmatrix} I_1 \\ I_2 \end{pmatrix} = \begin{pmatrix} Y_s & Y_m \\ Y_m & Y_s \end{pmatrix}\begin{pmatrix} V_1 \\ V_2 \end{pmatrix}. \tag{7}$$

Here, the self and mutual elements are given by:

$$Y_s(\omega) = \frac{1}{2}\left[\frac{1}{Z_e^+(\omega)} + \frac{1}{Z_e^-(\omega)}\right],$$
$$Y_m(\omega) = \frac{1}{2}\left[\frac{1}{Z_e^+(\omega)} - \frac{1}{Z_e^-(\omega)}\right], \tag{8}$$

where $Z_e^\pm$ are the equivalent one-port impedances for the superradiant (4) and subradiant (5) states, respectively. Thus, such impedances are given by (1), with the proper values of the resonance frequencies, $\omega_\pm$, and decoherences $\gamma_\pm$, corresponding to such two states (the detailed derivation of (8) is given in appendix B).

Relation (7) characterizes the two-port composed of two atoms in entangled state and interacting by the d-d interaction: it expresses the general relations between atom-field parameters. The mutual coupling expressed by the off-diagonal terms is a result of the quantum correlations, due the combination of the entanglement and d-d interaction, whose physical meaning becomes clear if one considers the Dicke-states $|\psi_\pm\rangle$ as excitons [63]. Indeed, the excitons in optical crystals [64] represent the electron-hole entangled states produced via the d-d interactions [5–13, 64]. Thus, the generalized Ohm's law in form (7) manifests the existence of excitons in electrical circuits. The non-locality in this case is analogous to the spatial dispersion in crystals [64].

The admittance matrix elements (8) characterize such conventional measure of entanglement as the Von Neumann entropy [65]. To show it, let us consider the excitation of the atom pair by the voltage V_1 applied to the first port. Due to the resonance condition $\omega \approx \omega_0$, only one of the two atoms may be excited with corresponding probability $p_{1,2}$, while another one appears in the ground state. As a result, corresponding currents will be induced in both ports. The Von Neumann entropy of the excited state is defined as

$$H_{V-N}(\omega) = -p_1(\omega)\log p_1(\omega) - p_2(\omega)\log p_2(\omega) \tag{9}$$

where

$$p_1(\omega) = \frac{|Y_s(\omega)|^2}{|Y_s(\omega)|^2 + |Y_m(\omega)|^2} \tag{10a}$$

and

$$p_2(\omega) = \frac{|Y_m(\omega)|^2}{|Y_s(\omega)|^2 + |Y_m(\omega)|^2} \tag{10b}$$

(for the proof of (10)—see appendix C). The Von Neumann entropy in accordance with (9), (10a, b) is strongly dependent on frequency. At the resonant frequencies of Dicke states $\omega = \omega_+$ and $\omega = \omega_-$, we have $p_1(\omega_\pm) = p_2(\omega_\pm) = 0.5$, and $H_{V-N}(\omega_\pm) = 1.0$, which correspond to the maximal entanglement of the excited state. Far from superradiant and subradiant resonances $H_{V-N}(\omega) \to 0$, which corresponds to the total disentanglement of the excited state.

3. Anomalous electromagnetic crosstalk via entanglement

In general, EMC problems are associated with undesirable mutual influence (coupling) between circuit elements. On the macroscale, the crosstalk noise between two circuit elements is a classical electromagnetic phenomenon, as a result of the EM-field penetration from one element into the other (and vice-versa). When the interaction is mainly due to the electric (magnetic) field penetration, the coupling is of capacitive (inductive) nature and is characterized by the effective mutual capacitances (inductances) [26–28]. At the nanoscale level, unusual crosstalk mechanisms may appear.

Before starting our analysis, let us dwell on the validity of the network concept. In general, lumped circuits are defined as systems all of whose components as well as the system as a whole are small compared to the wavelength (electrically small) [66, 67]. In this case, the field retardation is negligibly small. The electric and magnetic fields are confined inside the capacitors and inductors, respectively. Such elements are characterized by the primary parameters, which are variable independently, and every component may be even deleted from the circuit. On the other hand, validity of the equivalent circuit concept is not limited by the requirement of the small electrical size. This concept was formulated for microwave waveguides [68], cavities [68] and antennas [69] beyond the limitation of small electrical size. In our case, the equivalent circuit model can serve for both analysis and understanding of the electrical response of the quantum system. Here, equivalent currents excite the physical EM-fields in the spatial regions of interest. The problem is in correct definition and calculation of the effective parameters. In the case of electrically small systems, the parameter values are calculated via boundary-value problems of electrostatics or magnetostatics [66]. For more general cases, different heuristic and numerical techniques have been developed [66–69]. In principle, effective parameters may be found from experimental data. In such cases, effective inductances, capacitances and resistances are secondary parameters, which are not independent. As an example, consider the model of the atom discussed in the section 2.1 of this paper: the atomic primary parameters are the transition frequency and matrix element of dipole moment, while effective parameters are coupled, as follows from (3), by relations $C_e = \omega_0^{-2} L_e^{-1}$, $R_e = \gamma L_e$ and, thus not independently variable.

3.1. Crosstalk analysis

Let us consider the two quantum emitters analyzed in the previous section. We assume that one of them is 'active', i.e., it is connected to a voltage source V_0 through the corresponding electrode pair, hence $V_1 = V_0$, and the other is 'passive', for instance, the right end electrodes are left open (i.e., $I_2 = 0$). Let us define as crosstalk noise the voltage across the 'passive' emitter, i.e. $V_{XT} \equiv V_2|_{I_2=0}$. In contrast to classical EMC results, such a crosstalk is due both to classical electromagnetic coupling [24–26] and to the entanglement via the d-d interaction between the two atoms, i.e. quantum correlation.

To examine the role of the quantum correlation in the crosstalk phenomenon we have to take also into account the direct capacitive coupling between the two pairs of electrodes. To this end, we represent the overall system, i.e., the two coupled quantum emitters together with the two electrode pairs, through the equivalent π-type two-port depicted in figure 4. The contributions from the electrodes are taken into account though the

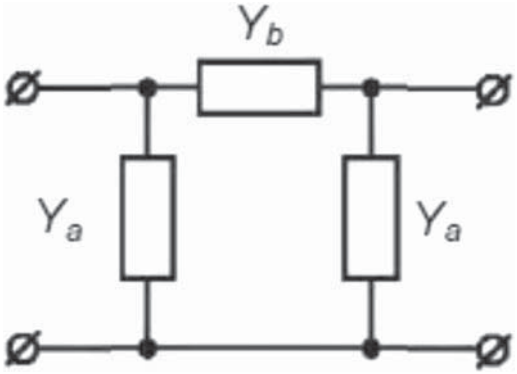

Figure 4. Equivalent symmetric π two-port of the pair of quantum emitters and electrodes shown in figure 3(a): $Y_a = (Z_e^+)^{-1} - i\omega C_{eg}$ and $Y_b = -Y_m - i\omega C_{LR}$, where C_{LR} is the capacitance between the two pairs of electrodes.

capacitance C_{eg} at each port (like that in figure 2(e)), and by an inter-electrode capacitance, C_{LR}, i.e. the capacitance between the two pairs of electrodes. Then, using (7) in classical synthesis formulas for a π-type two-port, it is easy to compute the element admittances in figure 4.

$$Y_a(\omega) = \frac{1}{Z_e^+(\omega)} - i\omega C_{eg},$$
$$Y_b(\omega) = -Y_m(\omega) - i\omega C_{LR}. \tag{11}$$

Only the super-radiant mode contributes to the admittance Y_a, while Y_b depends on both the super-radiant and sub-radiant modes. Two different mechanisms contribute to the admittance Y_b: the capacitive coupling associated in (11) with the capacitance C_{LR} and the quantum correlation between the two atoms, represented by the term Y_m.

Let us note that the load characteristics are very important in the crosstalk analysis. One of the main advantages of the developed technique is its independence of the type of the load. The electrodes on the right-hand-side of the π-type two-port depicted in figure 4 are left opened. An arbitrary linear load as well as the crosstalk area may be described by the admittance matrix. The total admittance matrix can be found as a product of the (normally ordered) partial admittance matrices [66]. The choice of the load allows to suppress or enhance the crosstalk level.

The crosstalk voltage V_{XT} is given by

$$V_{XT}(\omega) = \frac{Y_b(\omega)/Y_a(\omega)}{1 + (Y_b(\omega)/Y_a(\omega))} V_0(\omega), \tag{12}$$

therefore the amplitude of V_{XT} is strictly related to the admittance ratio Y_b/Y_a.

The two Dicke-states are characterized by different resonance frequencies, line-widths, and oscillation amplitudes, therefore, they can be excited separately. If $\Omega \gg \gamma_\pm$ and $\omega \approx \omega_+$ the inequality $|Z_e^+|^{-1} \gg |Z_e^-|^{-1}$ is fulfilled, and the contribution of the super-radiant mode to Y_m becomes dominant. In contrast, $\omega \approx \omega_-$ results in $|Z_e^+|^{-1} \ll |Z_e^-|^{-1}$ and the sub-radiant mode prevails. Therefore, for $\Omega \gg \gamma_\pm$ and $\omega \approx \omega_\pm$, we have $|Y_m(\omega_\pm)| \approx \omega_\pm \mu^2/\hbar\gamma_\pm A_{\text{eff}}$ and the mechanism that determines the crosstalk depends on the value of the ratio $r \equiv \omega_0 C_{e0}/2\gamma_\pm C_{LR}$. For $r \approx 1$, both the capacitive and quantum correlation couplings are important, whilst for $r \gg 1$, the quantum correlation contribution prevails (and vice-versa for $r \ll 1$). Let us consider the case $r \gg 1$, where $|Y_b(\omega_\pm)| \approx |Y_m(\omega_\pm)|$. Then according to (12), $|V_{XT}| \approx 0.5\ |V_0|$ for the super-radiant mode if $\omega_+ C_{eg} \ll |Y_m(\omega_+)|$, and $|V_{XT}| \approx |V_0|$ for the sub-radiant mode if $\omega_- C_{eg} \ll |Y_m(\omega_-)|$.

To keep our analysis general, we do not dwell on the specific shape of the electrodes and describe their effects in the crosstalk analysis via effective parameters of lumped components. However, the electrode shapes can significantly affect the distribution of the electromagnetic field. Also, at the frequencies involved, the length of interconnects becomes crucial. The experiment setup analysis should include propagation and transmission line effects on the interconnects, as well as matching, reflections, etc. To account for this effects, it is possible to consider each electrode as a segment of a microstrip line with quasi-TEM mode [68] and apply a well-developed technique [68] for the effective parameter calculation. The relevant inhomogeneities in the microstrip lines may be used as a framework for the analysis of inter-electrode coupling (for example, the coupling associated with the capacitance C_{LR} may be considered as a gap in the microstrip line [68]).

Ignoring the substrate effect is an additional approximation which has been made to simplify (6) for the Lamb shift. To account for the substrate influence, one can replace the free space dipole field by the field of the dipole located above the planar boundary of the dielectric [70]. In general, such field is rather complicated, but

may be simplified in the quasistatic limit $(\mathbf{k}\cdot\mathbf{r}_{12})\ll 1$ [70]. In this case, the Lamb shift approximately reads $\Omega\approx 2\vec{\mu}^2(1-3\cos^2\theta)/\pi\varepsilon_0\hbar(\varepsilon+1)^2|\mathbf{r}_{12}|^3$, where ε is the relative permittivity of the substrate. The Lamb shift depends on the distance between the two atoms and decreases as the distance increases. Nevertheless, the above behavior of the crosstalk voltage only depends on the key requirement $\Omega\gg\gamma_{\pm}$, hence we may have a strong crosstalk even for large interatomic distances. On the other hand, in the classical crosstalk mechanism (if we disregard the quantum correlation contribution to the crosstalk), the electromagnetic field penetration from one port to the other does not couple the atomic modes and strongly decreases with the interatomic distance: the value of admittance Y_a may strongly exceed that of Y_b.

If the impedances $Z_e^{\pm}$ become comparable, the amplitude of the coupling admittance Y_m becomes small and the quantum correlation contribution to the crosstalk becomes negligible. In the limit of zero Lamb-shift (6), the impedances Z_e^{+} and Z_e^{-} become equal and, as a result, the quantum correlation contribution to the crosstalk completely vanishes. Thus, the direct ways of anomalous crosstalk suppression are: (i) increasing the interatomic distance to achieve d-d quenching; (ii) artificial broadening of the atomic spectral lines via the introduction of additional losses (Q-factor degradation). These obvious ways are usually unsuitable from the nano-EMC point of view. The spatial separation assumes the availability of free space, which is not the case in many nanodevices. Decreasing the Q-factor often means the EMC problem is solved at the expense of their functional performance. Thus, it is important to develop special tools for the d-d suppression via the control of photonic density of states in the interatomic areas. As one of the striking examples, one can note the resonant photon exchange by atomic pairs in high-Q cavities, which has been considered in [41]. The atomic pair resonantly interacting with a high-Q cavity mode was considered in [41] as a set of three mutually coupled excited states (in contrast with two such states for the case of free space). It was shown, that the strong interference between the symmetric and anti-symmetric states (4), (5) leads to the single-atom states decoupling and corresponds to the suppression of interatom excitation transfer. Thus, the resonant interaction of the atomic pair with the virtual photons of high-Q cavity mode [41] may be considered as one of the promising tools for nano-device EMC decoupling. Coupling of a pair of distant atoms via a waveguide below cutoff [42] may be considered as an alternative approach for the suppression of the unwanted quantum crosstalk. No guiding photon modes exist in this case for interatomic exchange, thus the quantum component of electromagnetic crosstalk will be strongly suppressed in accordance with (8).

As predicted in [42], if initially only one atom is excited, we get a periodic exchange of the excitation between the atoms at a rate of Ω, which temporally modulates the interatomic entanglement. This physical mechanism is able to manifest itself in the regime of free oscillations. Let us consider a pair of the single atomic nanodevices coupled via the d-d interaction. Assuming that only the first atom is initially excited, the single atom functions are $|\Psi\rangle_1=A\,|e_1\rangle+B\,|g_1\rangle$, $|\Psi\rangle_2=|g_2\rangle$, where A, B are given probability amplitudes satisfying the normalization condition. The collective dynamics of the system are described by (B.4),(B.5). The exchange of the excitation [42] leads to a parasitic amplitude modulation of the observable currents $I_{1,2}(t)$ described by

$$\begin{pmatrix} I_1(t)\\ I_2(t)\end{pmatrix}\sim \mathrm{i}AB^{*}\mathrm{e}^{\mathrm{i}\omega_0 t}\begin{pmatrix}\omega_0 & \Omega\\ \Omega & \omega_0\end{pmatrix}\begin{pmatrix}\cos(\Omega t)\\ \mathrm{i}\sin(\Omega t)\end{pmatrix}+\mathrm{c.c.}, \tag{13}$$

This phenomenon is undesirable from the EMC point of view, because it produces unwanted additional spectral components. This transient process will be attenuated due to spontaneous emission, but the decay value $\gamma_{-}=\gamma-\gamma_{12}+\Gamma$ is rather weak due to the presence of the subradiant component in the collective state of the system (see (B.8)).

3.2. Anomalous crosstalk in lateral GaAs double quantum dot

Here we discuss a possible experiment designed to verify the concept of the anomalous electromagnetic crosstalk via entanglement developed above. In the optical range, we can use the lateral GaAs double quantum dot (DQD) within the two-dimensional electron gas of an AlGaAs/GaAs heterostructure with gold for metal electrodes, which has been proposed in [36] as a singlet-triplet qubit for quantum computing. The quantum interdot interaction in a DQD is produced by the exchange interaction, leading to a dipole-dipole entanglement of the ground and excited states [36]. The diode laser may be used for excitation as an external voltage source. The exchange interaction is controlled by varying the barrier height.

The experiment consists of the verification of the appearance of an ac-current in one of the QDs, denoted as 'passive', produced via entanglement by an ac-voltage source connected to the other QD, denoted as the 'active' one. The detection of this current may be performed by means of the emission of a nanoantenna attached to the passive QD. The ac-current is produced by the coherent dipole transitions in the DQD between the valence and conduction bands.

As pointed out above, the equivalent two-port model developed in section 2 accounts for both coupling via entanglement between the atomic states and the classical capacitive coupling. To demonstrate the quantum

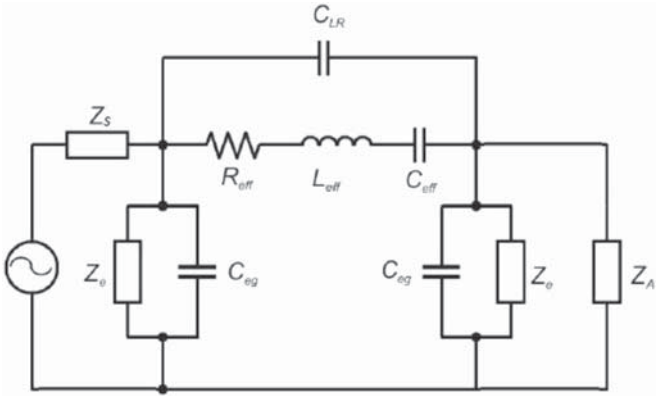

Figure 5. The equivalent circuit of the proposed experimental setup to observe anomalous crosstalk. A pair of two identical 'QD +gates' are connected on the left-side to an external voltage source and on the right-side to a nanoantenna. Here, Z_s represents the source impedance (possibly including the contribution of a nano-interconnect), and Z_A represents the nanoantenna radiation impedance (possibly including the impedance of a nano-interconnect). The two QDs are coupled via quantum entanglement and capacitive electric coupling and are modeled as in figure 4. The signal produced by the voltage source will be emitted through the antenna and measured by an external photodetector.

contribution to the crosstalk, entanglement needs to dominate over the capacitive coupling, which can occur subject to some key requirements.

The maximum contribution of quantum entanglement to the electromagnetic crosstalk is reached when the splitting of super-radiant and sub-radiant spectral lines exceeds their width, that is, 2Ω (given by (6)), must be sufficiently large compared to the line widths, $2\Omega \gg \gamma_+$. This condition is satisfied in the experimental configuration proposed in [71], where $\omega_0/2\pi \cong 10^{14}$ Hz. Indeed for two QDs separated by a GaAs barrier, the level splitting of the 1.26 eV line ($3 \cdot 10^{14}$ Hz) is 0.04 eV (i.e., $2\Omega/2\pi \cong 10^{13}$ Hz), while the decay time at T = 60 K is on the order of few picoseconds [72], which corresponds to a line-width of $\gamma_+ \cong 3 \cdot 10^{11}$ Hz. The linear dimension of the confinement area of the quantum dots is $a \approx 50 \div 80$ nm. An approximate value of the transition dipole moment is: $\mu \cong \sqrt{3\pi\varepsilon_0 \hbar c^3 \gamma/\omega_0^3}$ [55]. We consider the resonance with the superradiant mode, hence $\omega \approx \omega_0 + \Omega$. The ratio of the two components in (8) is given by $|Z_e^-(\omega_+)|/|Z_e^+(\omega_+)| \cong \gamma_+/4\Omega \cong 10^{-2}$, which guarantees the desired value of spectral line splitting (the first key requirement).

The equivalent circuit of the proposed experimental setup is presented in the figure 5: the two-port of figure 4 is augmented with the radiation impedance of a nanoantenna Z_A and the internal impedance of the voltage source Z_S. These two impedances possibly include the impedances of nano-interconnects to be used to connect these two elements to the two-port. Here, we have introduced the following effective coupling parameters, $L_{\text{eff}} = -(\omega^2 C_e/2)^{-1}$, $C_{\text{eff}} = -(2\omega^2 L_e)^{-1}$, and $R_{\text{eff}} = -2R_e$.

The second key requirement is that at the resonance frequency ω_+ the crosstalk in the DQD via the quantum entanglement should dominate over the capacitive coupling between the QDs, which is true if the interatomic distance S is sufficiently large. At the resonance frequency, the coupling admittance is given by $Y_m = 1/R_{eff}$. Therefore for an inter-atomic distance of 400 nm [36], we have $C_{LR} \cong 10^{-16}$F [36], which is low enough to satisfy $C_{LR} \ll (4\omega_0 |R_{eff}|)^{-1}$, i.e., to satisfy the second requirement. The crosstalk amplitude is maximized if $\omega_+ C_{LR} \ll R_e^{-1}$ (typically $C_{eg} \cong 10^{-16}$ F [73]).

Under these conditions, figure 6 presents the amplitude of the transfer function, $H = V_{\text{out}}/V_{\text{in}}$, defined as the ratio between the voltage $V_{\text{out}} = V_2$ exciting the antenna (assuming $|Z_A^{-1}| \ll |Z_e^{-1} - i\omega C_{eg}|$) and the voltage $V_{\text{in}} = V_1$ supplied by the voltage source. The considered values for the parameters are given in the figure 6 caption. The presence of a strong resonance peak around the transition frequency $f_+ = \omega_+/2\pi = 1.05 \cdot 10^{14}$ Hz is evident.

A similar experiment can also be performed at microwave frequencies using the exchange mechanism, which leads to entanglement both in the spin and the orbital parts of the DQD wave function [36]. The ac-current is produced by the coherent dipole quantum transitions in the DQD between the lowest energy state and the state that features one electron in the first excited orbital state. The allowed dipole transitions are between the states with identical spin parts of the wave function (singlet, or triplet ones) and correspond to $\omega_0/2\pi \cong 30$ GHz. In the low temperature regime (30 mK < T < 1 K), typical experimental values of the decay time are relatively large ($1 \div 200$ μs) [36, 73], thus likewise guaranteeing the fulfillment of the key requirements for the experimental implementation of the quantum crosstalk.

Let us note that the nanoantenna in figure 5 is represented by a parallel equivalent load in contrast to the series load in [44], but in agreement with [74]. The reason of such a discordance is the use of different definitions

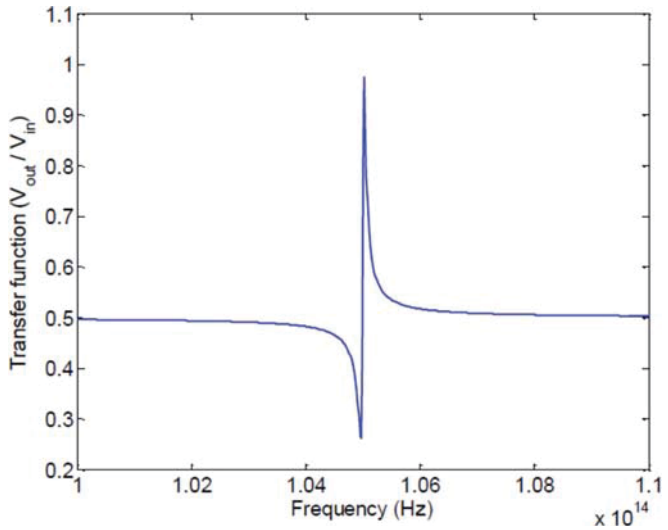

Figure 6. The amplitude of the transfer function for the proposed experimental setup, assuming $a = 80$ nm, $S = 400$ nm, $f_+ = 1.05 \cdot 10^{14}$ Hz, $\gamma_+ = 3 \cdot 10^{11}$ Hz, $\mu \cong 1.6 \cdot 10^{-26}$ Cm, $C_{LR} \cong C_{eg} = 10^{-16}$ F.

of antenna as an electronic device. Classically, antenna is defined as a device that transforms the near-field of the source to the free far-field (and vice-versa). It means that the source without antenna is assumed to be non-radiative. On the other hand, the external source in [44] is defined as a radiative dipole, while the antenna corresponds to the dipole environment, which enhances the radiation via scattering. Of course, the characteristic antenna impedances are given by various ways. We follow here the classical antenna theory [69] and use the Thévenin equivalent circuit.

Various types of optical nano-antennas have been developed for a variety of applications (for reviews—see, for example [31, 38–40]). For our purposes, a QD embedded in a top-down fabricated semiconductor nanowire antenna, recently implemented in [75] appears particularly promising. Such antenna composed of a segment of nanowire waveguide of diameter d with the fundamental EH_{11} mode ending in a conical taper introduced to allow adiabatical transition of the confined mode into a plane wave in free space. The design goals are to optimize both the coupling of the QD emission into the fundamental mode of the nanowire and the far-field radiation efficiency, defined in [75] as the ratio of power collected by an objective lens to the total power emitted from the QD. A *normalized nanowire diameter* (d/λ) of 0.235 was found to optimally funnel the QD emission into the antenna. For the optimal openning angle of the conical tapering, the efficiency reached $\eta > 50\%$.

Negative inductance/capacitance may be considered as a positive frequency dependent effective capacitance/inductance, respectively (see, for example, [29, 40]). Following [76], we can also consider the effective inductance/capacitance as a so-called left-handed medium with both permittivity and permeability being negative (Veselago-medium [77]). The negative resistance of the coupling element does not contradict the thermodynamic equilibrium. As noted by Schrödinger [1], the whole system can be less uncertain than either of its entangled parts. This means that the whole equivalent circuit is better specified than its elements. Thus, the negative resistance of a circuit element means that there is a special type of energy transfer inside the system, not supplied from outside. The appearance of negative resistance strongly contradicts the intuitive concepts of classical crosstalk, where the coupling channel of electromagnetic nature is represented by passive elements only [26–28].

It is important to note that the novel mechanism of crosstalk considered above is relevant only if the system is coherent (the coherent behavior for the states (4), (5) means that the probability to find one of the atoms in the ground/excited state is equal to the probability of finding another in the opposite state). In general, if the system in the excited state is left unperturbed, it evolves to the ground state due to the coupling with its environment (described as a bath) and loses its coherence and entanglement [65]. Such evolution is characterized by decoherence rate [65]). In contrast with digital processes in quantum informatics [65], we consider linear stationary oscillations supported by the external field. Therefore, the effect of decoherence manifests itself in the frequency properties of the admittance matrix (B.6) via Fourier integration in equation (B.1). The system does not lose its coherence, because it is continuously maintained by the external field (as a result, the Von Neumann entropy (9) is time independent). The effect of decoherence exhibits itself in the broadening of the spectral lines in equation (B.6) and in frequency dependence of the Von Neumann entropy. In this sense, the coherence corresponds to the ability to excite two spectral lines in the admittance matrix independently (the interline split

exceeds their widths). As discussed above, this condition, i.e. $\Omega \gg \gamma_{\pm}$, is practically achievable in currently realizable double QDs.

4. Summary and outlook

In this paper we have shown that an anomalous electromagnetic crosstalk may arise from the simultaneous existence of the electromagnetic interaction and quantum entanglement at the nanoscale. The main conclusions of the paper are as follows:

(1) As an efficient theoretical framework for nano-EMC analysis, the theory of electric circuits with quantum emitters (atoms) was proposed. For bridging the classical electric circuit theory with the quantum theory of nano-objects, the atoms inside nano-devices were described by their effective admittances. The effective admittance, classical in form but essentially of a quantum nature, is defined as a general susceptibility and calculated using the Kubo-technique. In order to account for decoherence the concept of effective Hamiltonian [21, 56, 57] was used, with the decoherence rates taken from experimental data;

(2) To illustrate the general concept, we have analyzed in detail the electromagnetic crosstalk between two identical electrical circuits, with identical two-level atoms in entangled states coupled via d-d interactions. The system was described in terms of an equivalent symmetric two-port. It was shown that the combination of entanglement and d-d interactions (quantum correlation) enables to change dramatically the physical picture of the crosstalk. In particular, in contrast with classical crosstalk [23–25], the excitation produced in one of the ports may be redistributed in equal parts between both of the ports, in spite of the rather small inter-atomic interaction, due to the quantum correlation;

(3) Depending on the specifics of the problem under consideration, one of the two mentioned mechanisms of crosstalk (classical electromagnetic crosstalk and quantum correlation) may be dominant or the two may be comparable. Control and suppression of the two types of crosstalk will require application of substantially different nano-EMC techniques. Thus, both of them should be taken into account *a-priori* in nanoelectronic design;

(4) A possible experimental implementation of the anomalous crosstalk via entanglement in the optical range has been proposed, based on a lateral GaAs double quantum dot.

Our work suggests a number of follow-up studies: (i) it is important to extend our consideration for other mechanisms of interatomic coupling and quantum entanglement (tunneling, spin-spin interactions, dissipative coupling via the common reservoir [78], noise coupling [79], etc), which allow the electromagnetic crosstalk of especially non-electromagnetic origin; (ii) it is important to investigate the equivalent circuits for multi-level and initially pumped quantum structures; (iii) it is important to account for decoherence using the theory of open quantum systems [80] (non-Markovian coupling of the system to the quantum bath [81, 82]).

Acknowledgments

This research was supported in part by the EU Horizon 2020 project H2020-MSCA-RISE-2014-644076 CoExAN and EU FP7 projects, FP7-PEOPLE-2012-IRSES-316432 QOCaN and FP7-PEOPLE-2013-IRSES-612285 CANTOR. Discussions of the basic ideas underlying this work with Dr S Starobinets and Dr D Mogilevtsev are acknowledged.

Appendix A. Effective admittance of a single two-level atom

Let us consider the interaction of a disk-like quantum dot with a classical monochromatic electric field $\mathbf{E} = \mathrm{Re}\{\mathbf{E}_0 \exp(-i\omega t)\}$. The ground and excited eigenstates are denoted by $|g\rangle$ and $|e\rangle$, respectively. The eigenstates for disk-like atom configuration are given by the Fock–Darwin model (2D-harmonic oscillator) [37]:

$$|g\rangle \Rightarrow \frac{1}{\sqrt{\pi}l}e^{-(x^2+y^2)/2l^2},$$
$$|e_x\rangle \Rightarrow \sqrt{\frac{2}{\pi l^4}}\,x e^{-(x^2+y^2)/2l^2},$$
$$|e_y\rangle \Rightarrow \sqrt{\frac{2}{\pi l^4}}\,y e^{-(x^2+y^2)/2l^2}, \tag{A.1}$$

where x and y are the plane Cartesian coordinates with the origin in the disk center, $l = \sqrt{\hbar/\omega_0 m_{\text{eff}}}$, ω_0 is the frequency of the harmonic oscillator and m_{eff} is an effective mass. Two excited states $|e_{x,y}\rangle$ are degenerate in energy and defined in (A.1) to ensure orthogonality. The dipole matrix element between $|g\rangle$ and $|e\rangle$ states is $\mu_x = \mu_y = \mu = \sqrt{2}\,l/4\pi$. It is independent of the direction in xy-plane due to the rotational symmetry of disk QD. Thus, we denote with $\hat{H}_a$ the atom Hamiltonian and with $\hat{H}_{\text{int}}$ the interaction Hamiltonian: $\hat{H}_a = \hbar(\omega_0 - i\gamma/2)(\hat{\sigma}_z/2)$; $\hat{H}_{\text{int}} = -e\hat{\sigma}\mu(\mathbf{e}\cdot\mathbf{E})$, where $\hat{\sigma} = \hat{\sigma}^+ + \hat{\sigma}^-$ with $\hat{\sigma}^+ = |e\rangle\langle g|$ and $\hat{\sigma}^- = |g\rangle\langle e|$, $\mathbf{e}$ is a unit vector in the xy-plane directed along the electric field.

We assume that the atom is initially prepared in the ground state, $|\psi(0)\rangle = |g\rangle$. An effective voltage is then defined as $V = -2a(\mathbf{e}\cdot\mathbf{E})$, where $2a$ is the linear size of the quantum confinement area. The effective current is defined as $I = -i\omega(\mathbf{e}\cdot\mathbf{p})/2a$. Taking into account that $\mathbf{p} = \alpha(\omega)\varepsilon_0\mathbf{E}$, where $\alpha(\omega)$is the polarizability and ε_0 is the vacuum-space permittivity, we can express the effective atom admittance as follows:

$$Y_e(\omega) \equiv \frac{I(\omega)}{V(\omega)} = \frac{i\alpha(\omega)\omega\varepsilon_0}{4a^2} = \frac{\omega\mu^2}{2\hbar A_{\text{eff}}}\int_0^\infty e^{i\omega t}\langle\hat{S}(\tau)\hat{S}(0) - \hat{S}(0)\hat{S}(\tau)\rangle\,d\tau, \tag{A.2}$$

where A_{eff} is the quantum confinement area. Here, the angle brackets mean the averaging over the ground state, whereas $\hat{S}(\tau)$ represents the operator $\hat{\sigma}$ in the interaction representation,

$$\hat{S}(\tau) = \hat{U}^T(\tau)\hat{\sigma}\hat{U}(\tau) \tag{A.3}$$

where

$$\hat{U}(t) = e^{i\hat{H}_a t/\hbar} = |g\rangle\langle g| + |e\rangle\langle e|e^{i(\omega_0 + i\gamma/2)t} \tag{A.4}$$

By using this relation, we obtain:

$$\hat{S}(\tau)\hat{S}(0) - \hat{S}(0)\hat{S}(\tau) = 2i\hat{\sigma}_z\sin(\omega_0\tau)e^{-\gamma t/2}, \tag{A.5}$$

where $\hat{\sigma}_z$ is the inversion operator, $\hat{\sigma}_z = |e\rangle\langle e| - |g\rangle\langle g|$. The next step is the substitution of (A.5) into (A.2) and the integration over τ. After a simple integration, we obtain the atom admittance

$$Y_e(\omega) = \frac{1}{Z_e(\omega)} = -i\frac{1}{\hbar A_{\text{eff}}}\frac{2\mu^2\omega\omega_0}{\omega_0^2 - \omega^2 - i\omega\gamma}. \tag{A.6}$$

The decoherence values for preliminary estimations may be taken from experimental data [47, 72, 75, 83].

Appendix B. Effective admittance matrix for the pair of atoms with d-d interaction

Let us now consider the quantum transitions stimulated by the classical monochromatic electric field $\mathbf{E} = \text{Re}\{\mathbf{E}_0\exp(-i\omega t)\}$ in the system composed of a pair of two-level disk-like quantum dots with dipole-dipole coupling (e.g., figure 1). The oscillations appear between the ground state $|g\rangle \equiv |g_1\rangle|g_2\rangle$ and both super-radiant and sub-radiant Dicke-states $|\psi_\pm\rangle$ given by (5). We have assumed that external field is off resonant with the transition between the ground state and the double excited state, $|e\rangle \equiv |e_1\rangle|e_2\rangle$, that is, $\omega \approx \omega_0$. As initial condition we will consider the ground state $|g\rangle$. Within the framework of the Kubo approach, the electric fields applied to both oscillators play the role of generalized perturbative forces, whereas the roles of the generalized responses are played by the induced dipole moments. The elements of the effective admittance matrices are given by

$$Y_{mn}(\omega) = \frac{\omega\mu^2}{2\hbar A_{\text{eff}}}\int_0^\infty e^{i\omega t}\langle\hat{S}_n(\tau)\hat{S}_m(0) - \hat{S}_m(0)\hat{S}_n(\tau)\rangle\,d\tau, \tag{B.1}$$

where $m, n = 1, 2$; the angle brackets always mean the averaging over the ground state. The operators $\hat{S}_n(\tau)$ represent the operator $\hat{\sigma}_n = \hat{\sigma}_n^+ + \hat{\sigma}_n^-$ in the interaction representation, $\hat{\sigma}_n^+ = |e_n\rangle\langle g_n|$, $\hat{\sigma}_n^- = |g_n\rangle\langle e_n|$,

$$\hat{S}_n(\tau) = \hat{U}^T(\tau)\hat{\sigma}_n\hat{U}(\tau) \tag{B.2}$$

and

$$\hat{U}(t) = e^{i(\hat{H}_a + \hat{H}_{dd})t/\hbar} = |g\rangle\langle g| + |\Psi_+\rangle\langle\Psi_+|\,e^{i(\omega_+ + i\gamma_+/2)t} + |\Psi_-\rangle\langle\Psi_-|\,e^{i(\omega_- + i\gamma_-/2)t} \tag{B.3}$$

The frequencies $\omega_{\pm}$ are separated by the collective Lamb shift (6), $\gamma_{\pm}$ being the decoherences of superradiant and subradiant modes with the ground state, respectively. Using the equalities $\hat{\sigma}_i^-\,|g\rangle = 0$, $\hat{\sigma}_1^+\,|g\rangle = |e_1, g_2\rangle$, $\hat{\sigma}_2^+\,|g\rangle = |g_1, e_2\rangle$, $\hat{\sigma}_1^+\,|\Psi_{\pm}\rangle = \pm|e_1, e_2\rangle/\sqrt{2}$, $\hat{\sigma}_2^+\,|\Psi_{\pm}\rangle = |e_1, e_2\rangle/\sqrt{2}$, $\hat{\sigma}_1^-\,|\Psi_{\pm}\rangle = |g\rangle/\sqrt{2}$ and $\hat{\sigma}_2^-\,|\Psi_{\pm}\rangle = \pm|g\rangle/\sqrt{2}$, we obtain

$$\hat{S}_n(\tau) = \hat{S}_s(\tau) - (-1)^n \hat{S}_a(\tau) \tag{B.4}$$

where

$$\hat{S}_s(\tau) = \frac{1}{\sqrt{2}}(|\Psi_+\rangle\langle g|\ \mathrm{e}^{\mathrm{i}\omega_+\tau} + |g\rangle\langle\Psi_+|\ \mathrm{e}^{-\mathrm{i}\omega_+\tau})\mathrm{e}^{-\gamma_+ t/2},$$
$$\hat{S}_a(\tau) = -\frac{1}{\sqrt{2}}(|\Psi_-\rangle\langle g|\ \mathrm{e}^{\mathrm{i}\omega_-\tau} + |g\rangle\langle\Psi_-|\ \mathrm{e}^{-\mathrm{i}\omega_-\tau})\mathrm{e}^{-\gamma_- t/2}. \tag{B.5}$$

By substituting (B.5) into (B.1) and integrating (in a similar way as done in appendix A), we obtain:

$$\mathbf{Y}(\omega) = -\frac{\mathrm{i}\omega\omega_+\mu^2}{A_{\mathrm{eff}}\hbar(\omega_+^2 - \omega^2 - \mathrm{i}\omega\gamma_+)}\begin{pmatrix}1 & 1\\ 1 & 1\end{pmatrix} - \frac{\mathrm{i}\omega\omega_-\mu^2}{A_{\mathrm{eff}}\hbar(\omega_-^2 - \omega^2 - \mathrm{i}\omega\gamma_-)}\begin{pmatrix}1 & -1\\ -1 & 1\end{pmatrix}, \tag{B.6}$$

As a consequence, we obtain

$$\mathbf{Y}(\omega) = \frac{1}{2Z_e^+(\omega)}\begin{pmatrix}1 & 1\\ 1 & 1\end{pmatrix} + \frac{1}{2Z_e^-(\omega)}\begin{pmatrix}1 & -1\\ -1 & 1\end{pmatrix}, \tag{B.7}$$

where the impedances $Z_e^{\pm}$ are given by (1), by using the proper values of the resonance frequencies, $\omega_{\pm}$, and of the decay rates of the excited levels, $\gamma_{\pm}$, corresponding to the superradiant and subradiant modes respectively. The values $\gamma_{\pm}$ are given by $\gamma_{\pm} = \gamma \pm \gamma_{12} + \Gamma$ [55], where γ and Γ are the spontaneous emission rate and the dephasing rate, respectively, and

$$\gamma_{12} = \frac{3}{2}\gamma\left\{\left[\frac{\sin x}{x} - \frac{\sin x}{x^3} + \frac{\cos x}{x^3}\right] + \cos^2\theta\left[\frac{3\sin x}{x^3} - \frac{3\cos x}{x^2} - \frac{\sin x}{x}\right]\right\}, \tag{B.8}$$

where all symbols are defined after (6) (see section 2).

The decay rate for preliminary estimations was taken from experimental data [47, 72, 75, 83]. For example, the dephasing measurements of the excitonic ground-state transition in a InGaAs/GaAs quantum dots were made in [83] using a highly sensitive four-wave mixing technique. The width and weight of the zero-phonon line in the homogeneous line shape are inferred from the measured polarization decay. The time evolution of the polarization amplitude of an individual resonance, i.e., the microscopic dephasing, is monitored by the time-integrated photon echo as a function of the delay time between the exciting pulses. The measurements have been implemented in the temperature range from 5 K to 120 K. After the initial non-exponential decay over a few picoseconds, a long exponential decay of the polarization was observed with a dephasing time inversely proportional to the width of the zero-phonon line. The experimental values of the decay rates corresponding to the pure dephasing via exciton-acoustic phonon interactions varied in the range of 0.1–100 μeV [83]. The radiative spectral line widths are measurable via non-resonant photo-luminescence spectroscopy, and their values are of the same order of magnitude [75].

Appendix C. Derivation of equation for Von Neumann entropy

In this appendix we will express the conditional probabilities $p_{1,2}$ to find the atoms 1, 2 in the excited state given that one of the atoms has been excited, in terms of the conductivity matrix (B.7). As follows from the definition of such conditional probabilities, the normalization condition $p_1 + p_2 = 1$ is fulfilled. Let us consider the temporal dynamics of the four-level system in the weak electromagnetic field depicted in figure 3. For simplicity, we will omit the decay rate in the intermediate calculations and introduce it again only at the final step. Such process, in general, may be described by the wavefunction

$$|\Psi(t)\rangle = C_g(t)|g_1\rangle|g_2\rangle + C_+(t)|\Psi_+\rangle + C_-(t)|\Psi_-\rangle + C_e(t)|e_1\rangle|e_2\rangle \tag{C.1}$$

where $C_{g,e}(t)$, $C_{\pm}(t)$ are unknowns. Let us assume that the system has been initially prepared in the ground state, thus the initial conditions are

$$C_g(0) = 1 \tag{C.2}$$
$$C_{\pm}(0) = C_e(0) = 0 \tag{C.3}$$

As it was shown in the appendix B, in the weak coupling limit that the value $C_e(t)$ is of the second order with respect to the coupling factor and therefore may be omitted. For the amplitude of the ground state probability we have approximately $C_g(t) \approx 1$. As a result, for the probability amplitudes of the Dicke-states we obtain from Schrödinger equation

$$\frac{dC_{\pm}}{dt} = -i\omega_{\pm}C_{\pm} + \frac{i\cos(\omega t)}{\sqrt{2}}(\Omega_{R1} \pm \Omega_{R2}) \tag{C.4}$$

where $\Omega_{R1,2}$ are Rabi-frequencies of the first and second atoms, respectively, which are proportional to the external voltages $V_{1,2}$. The forced oscillations component is

$$C_{\pm}(t) \approx \frac{(\Omega_{R1} \pm \Omega_{R2})}{2\sqrt{2}}\left(\frac{e^{-i\omega t}}{\omega - \omega_{\pm}} + \frac{e^{i\omega t}}{\omega + \omega_{\pm}}\right) \tag{C.5}$$

Let us assume that the voltage is applied only to the atom 1, while atom 2 is free ($\Omega_{R2} = V_2 = 0$). As follows from (B.6), the decay rate may be accounted by replacing $\omega^2 - \omega_{\pm}^2 \to \omega^2 - \omega_{\pm}^2 + i\omega\gamma_{\pm}$. As a result, (C.5) may be simplified to

$$C_{\pm}(t) \approx \frac{\Omega_{R1}}{2\sqrt{2}}\frac{e^{-i\omega t}}{\left(\omega - \omega_{\pm} + i\frac{\gamma_{\pm}}{2}\right)} \tag{C.6}$$

The wave-function may be rewritten in the next more convenient form:

$$|\Psi(t)\rangle \approx |g_1\rangle|g_2\rangle + D_1(\omega)|e_1\rangle|g_2\rangle e^{i\omega t} + D_2(\omega)|g_1\rangle|e_2\rangle e^{i\omega t}, \tag{C.7}$$

where $D_{1,2}(\omega) = (C_+(t) \pm C_-(t))e^{i\omega t}/\sqrt{2} \approx \sqrt{2}C_0 Y_{s,m}(\omega)$, $C_0 = aA_{\text{eff}}V_1/i\sqrt{2}\mu\omega_0$. The required probabilities are given by $p_{1,2} = |D_{1,2}|^2(|D_1|^2 + |D_2|^2)^{-1}$, which gives (10a, b). It is important to note, that the Von Neumann entropy (9) is defined only for the squared absolute values $|Y_{s,m}(\omega)|^2$, which means that this value is averaged over the external field oscillations.

References

[1] Schrödinger E 1935 *Naturwissenschaften* **23** 823
[2] Einstein A, Podolsky B and Rosen N 1935 *Phys. Rev.* **47** 777
[3] Cohen-Tannoudji C and Guery-Odelin D 2011 *Advances in Atomic Physics: an Overview* (Singapore: World Scientific)
[4] Dicke R H 1954 *Phys. Rev.* **93** 99
[5] Svidzinsky A A, Chang J T and Scully M O 2010 *Phys. Rev.* A **81** 053821
[6] Scully M O, Fry E C, Ooi C H R and Wo´dkiewicz K 2006 *Phys. Rev. Lett.* **96** 010501
[7] Svidzinsky A A, Chang J T and Scully M O 2008 *Phys. Rev. Lett.* **100** 160504
[8] Das S, Agarwal G S and Scully M O 2008 *Phys. Rev. Lett.* **101** 153601
[9] Scully M O 2009 *Phys. Rev. Lett.* **102** 143601
[10] Svidzinsky A A, Zhang X and Scully M O 2015 *Phys. Rev.* A **92** 013801
[11] Svidzinsky A A 2012 *Phys. Rev.* A **85** 013821
[12] Svidzinsky A A and Scully M O 2009 *Science* **325** 1510
[13] Wang D-W, Liu R-B, Zhu S-Y and Scully M O 2015 *Phys. Rev. Lett.* **114** 043602
[14] Meir Z, Schwartz O, Shahmoon E, Oron D and Ozeri R 2014 *Phys. Rev. Lett.* **113** 193002
[15] Röhlsberger R, Schlage K, Sahoo B, Couet S and Rüffer R 2010 *Science* **328** 1248
[16] Slepyan G Y and Boag A 2013 *Phys. Rev. Lett.* **111** 023602
[17] Mokhlespour S, Haverkort J E M, Slepyan G, Maksimenko S and Hoffmann A 2012 *Phys. Rev.* B **86** 245322
[18] Burkard G, Loss D and Di Vincenzo D P 1999 *Phys. Rev.* B **59** 2070
[19] Shinkai G, Hayashi T, Ota T and Fujisawa T 2009 *Phys. Rev. Lett.* **103** 056802
[20] Blais A, Huang R-S, Wallraff A, Girvin S M and Schoelkopf R J 2004 *Phys. Rev.* A **69** 062320
[21] Petrosyan D and Kurizki G 2002 *Phys. Rev. Lett.* **89** 207902
[22] Svidzinsky A A, Yuan L and Scully M O 2013 *Phys. Rev.* X **3** 041001
[23] Dhia S B, Ramdani M and Sicard E 2006 *Electromagnetic Compatibility of Integrated Circuits: Techniques for Low Emission and Susceptibility* (Berlin: Springer)
[24] Paul C R 1992 *Introduction to Electromagnetic Compatibility* (New York: Wiley)
[25] Ott H W 2009 *Electromagnetic Compatibility Engineering* (New York: Wiley)
[26] Slepyan G, Boag A, Mordachev V, Sinkevich E, Maksimenko S, Kuzhir P, Miano G, Portnoi M E and Maffucci A 2014 *Proc. of IEEE Intern. Conf, on EMC (Tokyo, Japan)* EMC 14, paper # 13A1-H4 13–6
[27] Slepyan G, Boag A, Mordachev V, Sinkevich E, Maksimenko S, Kuzhir P, Miano G, Portnoi M E and Maffucci A 2015 *Proc. of IEEE Intern. Conf. on Nanotechnology (Roma, Italy, 27–30 July)* IEEE NANO-2015, paper #420 184–7
[28] Slepyan G, Boag A, Mordachev V, Sinkevich E, Maksimenko S, Kuzhir P, Miano G, Portnoi M E and Maffucci A 2015 *IEEE Trans. on Electromagnetic Compatibility* **57** 1645
[29] Engheta N, Salandrino A and Alu A 2005 *Phys. Rev. Lett.* **95** 095504
[30] Maffucci A, Miano G and Villone F 2005 *IEEE Trans. on Advanced Packaging* **28** 174
[31] Agio M and Alu A 2013 *Optical Antennas* (Cambridge: Cambridge University Press)
[32] Bergman D J and Stockman M I 2003 *Phys. Rev. Lett.* **90** 027402
[33] Chen X-W, Agio M and Sandoghdar V 2012 *Phys. Rev. Lett.* **108** 233001
[34] Shchegrov A V, Joulain K, Carminati R and Greffet J-J 2000 *Phys. Rev. Lett.* **85** 1548
[35] Nemilentsau A M, Slepyan G Y and Maksimenko S A 2007 *Phys. Rev. Lett.* **99** 147403
[36] Kornich V, Kloeffel C and Loss D 2014 *Phys. Rev.* B **89** 085410
[37] Duan F and Guorin J 2007 *Introduction to Condensed Matter Physics* vol 1 (Singapore: World Scientific)
[38] Biagioni P, Huang Y-S and Hecht B 2012 *Rep. Prog. Phys.* **75** 024402
[39] Novotny L and van Hulst N 2011 *Nat. Photon.* **5** 83
[40] Engheta N 2007 *Science* **317** 1698

[41] Kurizki G, Kofman A G and Yudson V 1996 *Phys. Rev.* A **53** R35
[42] Shahmoon E and Kurizki G 2013 *Phys. Rev.* A **87** 033831
[43] Shahmoon E and Kurizki G 2014 *Phys. Rev.* **89** 043419
[44] Greffet J-J, Laroche M and Marquir F 2010 *Phys. Rev. Lett.* **105** 117701
[45] Todorov Y and Sirtori C 2014 *Phys. Rev.* X **4** 041031
[46] Landauer R 1957 *IBM Journ. Res. Dev.* **1** 223
[47] Valente D C B, Mucciolo E R and Wilhelm F K 2010 *Phys. Rev.* B **82** 125302
[48] Gabelli J, Feve G, Berroir J-M, Placais B, Cavanna A, Etienne B, Jin Y and Glattli D C 2006 *Science* **313** 499
[49] Chorley S J, Wabnig J, Penfold-Fitch Z V, Petersson K D, Frake J, Smith C G and Buitelaar M R 2012 *Phys. Rev. Lett.* **108** 036802
[50] Kubo R, Toda M and Hashitsume N 1985 *Statistical Physics (vol II. Non-equilibriume Statistical Mechanics* (Berlin: Springer)
[51] Landau L D and Lifshitz E M 1980 *Statistical Physics (Course of Theoretical Physics)* vol 5 (New York: Pergamon)
[52] Landau L D and Lifshitz E M 1981 *Quantum Mechanics. Non-Relativistic Theory (Course of Theoretical Physics)* vol 3 (New York: Pergamon)
[53] Van der Wiel W G, De Franceschi S, Elzerman J M, Fujisawa T, Tarucha S and Kouwenhoven L P 2003 *Rev. Mod. Phys.* **75** 1
[54] Scully M O and Zubairy M 2001 *Quantum Optics* (Cambridge: Cambridge University Press)
[55] Agarwal G S 2013 *Quantum Optics* (Cambridge: Cambridge University Press)
[56] Craig D P and Thirunamachandran T 1984 *Molecular Quantum Electrodynamics* (London: Academic)
[57] Lehmberg R H 1970 *Phys. Rev.* A **2** 883
[58] Ficek Z and Tanas R 2002 *Phys. Rep.* **372** 369
[59] Gillet J, Agarwal G S and Bastin T 2010 *Phys. Rev.* A **81** 013837
[60] Gea-Banacloche J, Mumba M and Xiao M 2006 *Phys. Rev.* B **74** 165330
[61] Urban E *et al* 2009 *Nat. Phys.* **5** 110
[62] Gaëtan A *et al* 2009 *Nat. Phys.* **5** 105
[63] Chen Y N, Chuu D S and Brandes T 2003 *Phys. Rev. Lett.* **90** 166802
[64] Agranovich V M and Ginzburg V L 1984 *Crystal Optics with Spatial Dispersion, and Excitons* (Berlin: Springer)
[65] Nielsen M and Chuang I 2012 *Quantum Computation and Quantum Information* (Cambridge: Cambridge University Press)
[66] Harrison R F 1961 *Time-Harmonic Electromagnetic Fields* (New York: Wiley)
[67] Voltmer D 2007 *Fundamentals of Electromagnetics 2: Quasistatics and Waves* (Morgan & Claypool)
[68] Montgomery C D, Dicke R H and Parcell E M (ed) 1948 *MIT Radiation Laboratory Series* vol 8 (New York: McGraw-Hill Book Company)
[69] Balanis K 2005 *Antenna Theory* (New York: Wiley)
[70] Novotny L and Hecht 2006 *Principles of Nano-Optics* (Cambridge: Cambridge University Press)
[71] Bauer M *et al* 2001 *Science* **291** 453
[72] Blick R H, Pfannkuche D, Haug R J, Klitzing K V and Eberl K 1998 *Phys. Rev. Lett.* **80** 4032
[73] Rabl P, Kolkowitz S J, Koppens F H L, Harris J G E, Zoller P and Lukin M D 2010 *Nature Phys.* **6** 602
[74] Alu A and Engheta N 2008 *Phys. Rev. Lett.* **101** 043901
[75] Kremer P E *et al* 2 *014 Phys. Rev.* B **90** 201408(R)
[76] Caloz A and Itoh T 2004 *IEEE Trans. Antennas and Propagation* **52** 1159
[77] Veselago V G 1968 *Sov. Phys. Uspekhi* **10** 509
[78] Mogilevtsev D, Slepyan G Y, Garusov E, Kilin S Y and Korolkova N 2015 *New J. Phys.* **17** 043065
[79] Mogilevtsev D and Slepyan G Y 2016 *Phys. Rev.* A **94** 012116
[80] Breuer H-P and Petruccione F 2002 *The Theory of Open Quantum Systems* (Oxford: Clarendon)
[81] Mogilevtsev D, Nisovtsev A P, Kilin S, Cavalcanti S B, Brandi H S and Oliveira L E 2008 *Phys. Rev. Lett.* **100** 017401
[82] Calarco T, Datta A, Fedichev P, Pazy E and Zoller P 2003 *Phys. Rev.* A **68** 012310
[83] Borri P, Langbein W, Woggon U, Jensen J R and Hvam J M 2005 *Phys. Rev.* **63** 035307